Design of Real-Time Measurement System with Vision/IMU for Close-Range Semi-Physical Rendezvous and Docking Simulation

Zhenshen Qu, Xiangyu Chu, Mengyu Fu, Xiaokai Liu, Weinan Xie and Changhong Wang

Abstract—**Design of a real-time measurement system based on information fusion of Vision Measurement Unit (VMU) and Inertial Measurement Unit (IMU) is proposed for a semi-physical simulation system. Main contributions of the paper are the design and application of VMU-IMU integration to the real-time simulation of close-range rendezvous and docking (RVD) in lunar orbit. Structure and each component of the system are presented. The pose (position and attitude) filters utilized for information fusion within Kalman filter (KF) framework are designed, which regard Hill equations and quaternion differential equations as process models respectively and choose relative pose of two spacecraft as measure variables. Capabilities of the real-time measurement system are demonstrated by semi-physical closed-loop simulations, which show the proposed system yields more precise navigation result and more effective preservation of energy than an independent VMU.**

I. Introduction

With Chinese unmanned explorer "Chang E-3" realizing a soft-landing on the Moon for the first time, Chinese lunar exploration project has been steadily implemented [1]. Subsequently, an assignment in this project is to send a sample canister back to Earth. It is a critical technique in sample return mission to carry out automated rendezvous and docking (RVD) of a chaser spacecraft with respect to a target spacecraft in lunar orbit. A hardware-in-the-loop simulation system, served to test the Guidance, Navigation and Control (GNC) System, is given to simulate the process of the RVD and comes to be more reliable than the numerical simulation. Precision of pose measurements between the chaser and the target will be of vital value for success of autonomous proximity operation, especially for the circumstance of close-range distance. Therefore, the real-time measurement system is the key part of the semi-physical simulation system.

The research on close-range measurement has gained much attention. F. J. Pelletier introduced a simulation of an autonomous rendezvous in Mars orbit. The relative orbit determination was carried out by processing chaser-to-target range and bearing data as observed by a scanning LIDAR instrument [2]. In [3], a study on the use of flash LIDAR for relative pose and trajectory estimation was presented, and the close approach results were focused on processing feature based tracking into relative attitude and translation measurements. J. F. Shi proposed a pose estimation method for autonomous robotic proximity operations with an uncooperative target, using a single infrared camera and a simple three-dimensional model of the target [4]. F. Sansone employed the 2D short-range navigation sensor for cooperative spacecraft, which exploited an infrared LED transmitter mounted on the target and two photodiode receivers mounted on the chaser [5].

In this work, real-time measurement system is designed for an autonomous RVD in lunar orbit. Obviously, there is no one involved in this activity temporarily, and the long distance makes the ability of real-time control from the ground station weakened, so the automation and autonomy of the RVD is demanded to be enhanced greatly [6]. According to this demand, it is necessary to fuse different types of sensor information for higher accuracy of navigation. Generally, gyros and accelerations are the typical sensors for absolute pose measurements, while cameras are for relative. Consequently, the real-time measurement system focuses on the implementation of fusing the measurements from an inertial measurement unit (IMU) and a double-camera vision sensor.

Due to the characteristics of cameras, they only have the capacity of detecting relative position and attitude information, but no access to relative speed and angular velocity directly. And the pose measurements of cameras are mingled with some noise. These defects may deteriorate the accuracy of relative pose determination and cause fuel waste, when simply using cameras to achieve closed-loop control for the RVD [7]. The measurements from the IMU perform high accuracy in a short period of time, which is capable of providing navigation reference. Unfortunately, owing to its full autonomy, error accumulation of the IMU exists. In order to solve this problem, the information fusion algorithm based on vision and inertial information is projected. Inertial information provides a reference for vision-only navigation, and vision information compensates the cumulative error for inertial navigation. Finally, the feasibility of information fusion algorithm was verified by numerical simulation, and the closed-loop semi-physical experiment was accomplished in a semi-physical simulation system. The results show that the real-time measurement system is capable of not only meeting the requirements of the control precision of the RVD, but also helping to improve navigation precision and save fuels effectively.

II. Design of the Semi-Physical Simulation System

A. System Composition

The semi-physical simulation system for an autonomous RVD mainly includes the central control console (CCC), physical simulation subsystem (PSS), dynamics simulation

*Resrach supported by the National Natural Science Foundation of China (61375046, 61403095)

Zhenshen Qu, Xiangyu Chu, Mengyu Fu, Xiaokai Liu, Weinan Xie and Changhong Wang are with Department of Control Science and Engineering, Harbin Institute of Technology, Harbin, 150001 China. Xiangyu Chu is the corresponding author (e-mail: chuxiangyu03@163.com).

978-1-4673-8318-9/16/$31.00©2016 IEEE

subsystem (DSS), data management subsystem (DMS), and integrated control subsystem (ICS), etc., as shown in Fig. 1 [8].

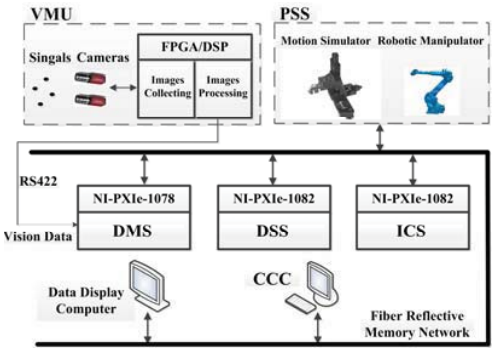

Figure 1. Composition of the semi-physical simulation system

Vision measurement unit (VMU) and PSS are material objects, while the other subsystems are running on the real-time simulation computers. The PSS consists of six DOFs motion simulator and three DOFs robotic manipulator, and they simulate the chaser and the target respectively. Three DOFs translating movement of motion simulator is imitated by driving motors and rails, and other three DOFs for rotating movement are accomplished by a three-axis turntable. The robotic manipulator fixed with markers is required to be static. The DSS contains the kinematics and vehicle dynamics for six DOFs, and an interference model derived from the non-spherical gravitation of the Moon, the gravity gradient and the perturbation of solar array, which is adopted to simulate spacecrafts' status and situations. The ICS is to guide and control the chaser for achieving the purpose of safe docking. Its ingredients include a filter module, a trajectory planning module and a controller.

The premise of the semi-physical simulation is to achieve real-time simulation that primarily relies on real-time simulation computers. PXIe-1078, PXIe-1082 and the corresponding system controller supplied by the National Instruments (NI) are as the hardware for the real-time simulation. The DSS and the GNC System are run in two sets of NI real-time simulation computer, which depend on a fiber reflective memory network (FRMN) for data transmission. The bold black lines in Fig. 1 represent the signal flow based on the FRMN. When the data is written into a reflective memory card, it will be automatically transmitted to other memory cards of the network, achieving the goal of data sharing. Because of no need to obey multilevel communication protocols, there is almost no delay caused by software, which ensures real-time working. The fiber reflective memory cards GE5565 PIORC produced by the General Company (GE) are chosen in this work.

B. Real-Time Measurement System

Real-time measurement system plays a significant role in semi-physical simulation system. It works as the feedback in a closed-loop system. It is composed of an IMU, a VMU and an information fusion algorithm.

The IMU contains a fiber optic gyro and a quartz flexible accelerometer, however, the virtual IMU is employed in this system. Seeing that gyros and accelerometers have accumulated error in working time, the analyses of their error models are utilized for compensation, as shown below,

$$\boldsymbol{U}_g = \boldsymbol{\omega} + \boldsymbol{\varepsilon} + \boldsymbol{v}_g, \ \dot{\boldsymbol{\varepsilon}} = \boldsymbol{v}_\varepsilon , \tag{1}$$

$$\boldsymbol{U}_a = \boldsymbol{f} + \boldsymbol{d} + \boldsymbol{v}_a, \ \dot{\boldsymbol{d}} = \boldsymbol{v}_d . \tag{2}$$

In (1), $\boldsymbol{U}_g$ is the measurement vector of gyros. $\boldsymbol{v}_g$, $\boldsymbol{\varepsilon}$ and v_ε are the gyros' measurement noise, drifts and rate noise respectively. And $\boldsymbol{\omega}$ is the angular speed of a vehicle in inertial space, expressed in its body-fixed reference frame. In (2), $\boldsymbol{U}_a$ is the output vector of accelerometers. $\boldsymbol{v}_a$, $\boldsymbol{d}$ and $\boldsymbol{v}_d$ are the accelerometers' measurement noise, bias and rate noise respectively. And $\boldsymbol{f}$ is the specific force in the vehicle's body-fixed reference frame. All the noise is assumed to be zero-mean Gaussian and white.

The VMU consists of the following functional elements.

- The chaser mounts a set of CMOS binocular-cameras, whose chips are Star1000. They can take digital images of the target.
- The infrared indicator is installed on the target, consisted of six LEDs uniformly distributed on a circle, which act as reference to the VMU.
- The data processing module, including FPGA and DSP, acquires the images from cameras and then processes them for determining relative position and orientation of the two spacecraft. After having performed in image processing, the module transmits the data to the DMS via the RS422 network, as depicted in Fig 1.

Detail of camera's relative measurement algorithm is not the topic in the paper. In the numerical simulation, it is assumed that relative position and attitude of the two spacecraft from the VMU can be used directly, and the outputs of the VMU are usually simplified to true relative pose information attached with zero-mean Gaussian and white-noise.

C. Closed-Loop Configuration

On the basis of the existing semi-physical simulation system, the closed loop is designed to test the performance of the real-time measurement system, as shown in Fig. 2.

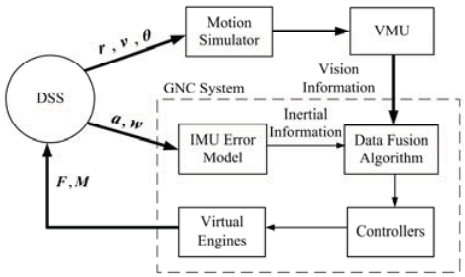

Figure 2. Closed loop for the semi-physical simulation

According to Fig. 2, the work principle is explained as follows.

- The motion simulator mainly receives position $\boldsymbol{r}$, velocity $\boldsymbol{v}$ and attitude angle $\boldsymbol{\theta}$ from the DSS for imitation of six DOFs motion of the chaser. The cameras mounted on motion simulator provide images for the data processing module of the VMU, which can gain vision information, i.e., relative pose of the two spacecraft.
- The DSS exports the acceleration $\boldsymbol{a}$ and angular velocity $\boldsymbol{\omega}$ of the chaser to the GNC System. They are transformed into virtual inertial information through the IMU error model, i.e., (1) and (2).
- Both vision information and virtual inertial information are input to the fusion filter module based on data fusion algorithm, which is able to improve the precision of navigation parameters.
- The control deviations, originated from the difference of fused values and expected values, are imported to the controllers. The control signals from controllers are transformed into thrust commands, a set of two digital signals with values "1" and "0". "1" represents the thrusters working, while "0" denote the thrusters closed.
- The control force $\boldsymbol{F}$ and control torque $\boldsymbol{M}$ calculated from the virtual engines are input to the DSS as a feedback.

This system chiefly adopts the LabVIEW Real-Time operating system, and it is an extended module for the real-time application of LabVIEW programs. The external development system of LabVIEW RT is LabVIEW. Its functions are developing and debugging real-time programs in a non-real-time system, like the Windows operating system. Software development usually uses interactive programming of MATLAB/Simulink and LabVIEW, i.e., model building is completed by using MATLAB firstly, and then the MTALAB files are generated into a dynamic link library (DLL), finally the DLL is downloaded to the real-time simulation computers.

III. Principle of Information Fusion

The VMU described in section II, has the ability to measure relative attitude and position of the target with respect to the chaser. Nevertheless, these measurements are mixed up with certain noise that lead to redundant pose control of the chaser, and they do not include the changing rate of pose. In order to compensate for these limitations, both the measurements of the IMU and the outputs of the VMU are exploited to aid in state estimation of the chaser. However, the gyro and accelerometer information is influenced by drift and bias. As a result, Kalman filters are adopted to fuse the information from the VMU and IMU. Particularly, two filters are implemented, as shown in Fig. 3. The first one, called attitude Kalman filter (AKF), deals with the rotation motion, while the other one, called position Kalman filter (PKF), copes with the translational motion [9]. Note that the Acc. is the Abbreviations of accelerometer.

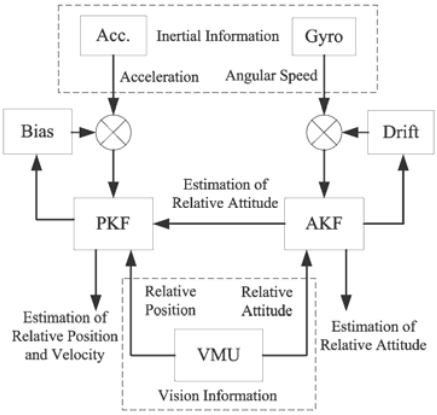

Figure 3. Block diagram of the information fusion algorithm

A. Reference Frames

Throughout this paper, the following coordinate systems that keep to right-hand rule are used to set up filters, as shown in Fig. 4. $\{i\}$, $\{H\}$ and $\{c\}$ denote selenocentric reference frame, orbital reference frame and chaser reference frame respectively.

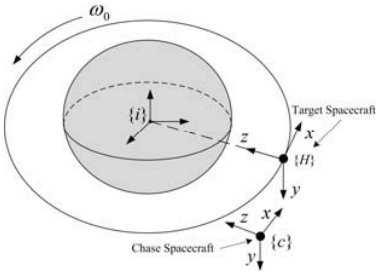

Figure 4. Co-ordinate of spacecraft rendezvous

B. Attitude Kalman Filter

Assuming that the Hill frame is regarded as reference frame, the quaternion differential equations used for depicting the evolution of relative attitude motion of the chaser is

$$d\boldsymbol{Q}/dt = 0.5\Omega\left(\boldsymbol{\omega}_{Hc}^{c}\right)\boldsymbol{Q}\text{, where } \boldsymbol{\omega}_{Hc}^{c} = \boldsymbol{\omega} - \boldsymbol{R}_{H}^{c}\boldsymbol{\omega}_{iH}^{H}, \tag{3}$$

and $\boldsymbol{Q}$ is the quaternion from $\{H\}$ to $\{c\}$, i.e., $\boldsymbol{Q} = q_1\boldsymbol{i} + q_2\boldsymbol{j} + q_3\boldsymbol{k} + q_4$, $\boldsymbol{\omega}_{Hc}^{c}$ is the angular velocity of $\{c\}$ with respect to $\{H\}$ expressed in the frame $\{c\}$, $\Omega\left(\boldsymbol{\omega}_{Hc}^{c}\right)$ is the skew-symmetric matrix determined by $\boldsymbol{\omega}_{Hc}^{c}$. $\boldsymbol{\omega}_{iH}^{H}$, expressed in $\{H\}$ with $\begin{bmatrix}0 & -\omega_0 & 0\end{bmatrix}^T$, represents the inertial angular velocity of the $\{H\}$, where ω_0 is a constant for orbital angular velocity. $\boldsymbol{R}_{H}^{c}$ is a direct cosine matrix transforming from $\{H\}$ to $\{c\}$. Now the state vector is defined as

$$\boldsymbol{x} = \begin{bmatrix} q_1 & q_2 & q_3 & q_4 & \varepsilon_x & \varepsilon_y & \varepsilon_z \end{bmatrix}^T, \tag{4}$$

where $\boldsymbol{\varepsilon} \in \mathbb{R}^3$ is the gyro drift. Equation (1) and (3) can be combined in the nonlinear form as $\dot{\boldsymbol{x}} = \boldsymbol{f}\left(\boldsymbol{x}, \boldsymbol{w}\right)$, which is

applied for state propagation. However, the Kalman filter is just for linear system. Linearizing the nonlinear equation yields the continuous-time process model

$$\dot{\boldsymbol{x}} = \boldsymbol{F}\boldsymbol{x} + \boldsymbol{G}\boldsymbol{w}\,, \tag{5}$$

where the state-transition matrix $\boldsymbol{F} = \partial \boldsymbol{f} / \partial \boldsymbol{x}$ is expressed as below

$$\begin{aligned} &\boldsymbol{F}_{11} = 0.5\left(\Omega\left(\boldsymbol{\omega}_{Hc}^{c}\right) + \omega_0 \cdot \boldsymbol{A}\right),\ \boldsymbol{F}_{21} = \boldsymbol{0}_{3\times 4} \\ &\boldsymbol{F}_{12} = 0.5\begin{bmatrix} -q_4 & q_3 & -q_2 \\ -q_3 & -q_4 & q_1 \\ q_2 & -q_1 & -q_4 \\ q_1 & q_2 & q_3 \end{bmatrix},\ \boldsymbol{F}_{22} = \boldsymbol{0}_{3\times 3} \end{aligned}\,. \tag{6}$$

and $\boldsymbol{G} = \left[\boldsymbol{F}_{12}\ \ \boldsymbol{0}_{4\times 3}; \boldsymbol{0}_{3\times 3}\ \ \boldsymbol{I}_{3\times 3}\right]$. Note that the matrix $\boldsymbol{A}$ is so complicated that there will be no showing. Considering the discrete-time, the process model can be written as follow

$$\boldsymbol{x}_{k+1} = \boldsymbol{\Phi}_{k+1,k}\boldsymbol{x}_k + \boldsymbol{\Gamma}_{k+1,k}\boldsymbol{w}_k\,, \tag{7}$$

where $\boldsymbol{\Phi}_{k+1,k} = e^{\boldsymbol{F}_k T_s} \approx \boldsymbol{I} + T_s \boldsymbol{F}_k$ and $\boldsymbol{\Gamma}_{k+1.k} \approx T_s \cdot \boldsymbol{G}_k$ with T_s being sampling time. The process noise $\boldsymbol{w}_k$ generally resembles Gauss white noise, which satisfies $E\left[\boldsymbol{w}_k\right] = \boldsymbol{0}$, $E\left[\boldsymbol{w}_k \boldsymbol{w}_j^{\mathrm{T}}\right] = \boldsymbol{Q}_k \delta_{kj}$ and $\boldsymbol{Q}_k = \mathrm{diag}\left[\sigma_{gx}^2\ \sigma_{gy}^2\ \sigma_{gz}^2\ \sigma_{\varepsilon x}^2\ \sigma_{\varepsilon y}^2\ \sigma_{\varepsilon z}^2\right]$.

Based on the outputs of the VMU, the measurement variables are chosen as

$$\boldsymbol{z} = \left[\theta_1\ \ \theta_2\ \ \theta_3\right]^T\,, \tag{8}$$

where $\boldsymbol{\theta} \in \mathbb{R}^3$ is the relative attitude of $\{c\}$ with respect to $\{H\}$. Due to the relationship between quaternion and Euler angles, the measurement variables can be expressed in terms of the state variables. It is clear that

$$\begin{cases} \theta_1 = \arctan\dfrac{2\left(q_1 q_4 + q_2 q_3\right)}{-q_1^2 - q_2^2 + q_3^2 + q_4^2} \\ \theta_2 = \arcsin\left[2\left(q_2 q_4 - q_1 q_3\right)\right] \\ \theta_3 = \arctan\dfrac{2\left(q_3 q_4 - q_1 q_2\right)}{q_1^2 - q_2^2 - q_3^2 + q_4^2} \end{cases}\,. \tag{9}$$

Thus, the observation equation can be written as

$$\boldsymbol{z} = \boldsymbol{h}\left(\boldsymbol{x}\right) + \boldsymbol{v}\,, \tag{10}$$

where $\boldsymbol{v}$ is the observation noise, which is supposed to be white with covariance $E[\boldsymbol{v}\boldsymbol{v}^T] = \boldsymbol{R}$. Obviously, (10) is a nonlinear function. The sensitivity matrix $\boldsymbol{H}$ can be derived by $\boldsymbol{H} = \partial \boldsymbol{h} / \partial \boldsymbol{x}$. And the observation noise covariance is $\boldsymbol{R}_k = \mathrm{diag}\left[\sigma_{\theta 1}^2, \sigma_{\theta 2}^2, \sigma_{\theta 3}^2\right]$.

C. Position Kalman Filter

Assume that the target spacecraft remains attitude stabilization and it follows a Keplerian orbit. According to the linearized Clohessy and Wiltshire equations [10], the relative kinematic equation of the chaser with respect to the target expressed in $\{H\}$ can be written as

$$\begin{cases} \ddot{x}^H - 2\omega_0 \dot{z}^H = f_x^H \\ \ddot{y}^H + \omega_0^{\ 2} y^H = f_y^H \\ \ddot{z}^H + 2\omega_0 \dot{x}^H - 3\omega_0^2 z^H = f_z^H \end{cases}\,, \tag{11}$$

where f_x^H, f_y^H and f_z^H are the component of control acceleration of the spacecraft in $\{H\}$. The $\boldsymbol{f}^H$ is related by $\boldsymbol{f}^H = \boldsymbol{f}_{ic}^H = \boldsymbol{R}_c^H \boldsymbol{f}_{ic}^c$, where $\boldsymbol{f}_{ic}^c$ is the specific force of the chaser and $\boldsymbol{R}_c^H = \boldsymbol{R}_H^{c\,T}$. Now assume that the state vector to be estimated is

$$\boldsymbol{x} = \left[x^H\ y^H\ z^H\ \dot{x}^H\ \dot{y}^H\ \dot{z}^H\ d_x\ d_y\ d_z\right]^T\,, \tag{12}$$

where $\boldsymbol{d} \in \mathbb{R}^3$ is the accelerometer bias. Equation (2) and (11) make up the system model, expressed by

$$\dot{\boldsymbol{x}} = \boldsymbol{F}\boldsymbol{x} + \boldsymbol{B}\boldsymbol{x} + \boldsymbol{G}\boldsymbol{w}\,. \tag{13}$$

The following quantities are substituted in (13).

$$\begin{aligned} &\boldsymbol{F} = \begin{bmatrix} \boldsymbol{0}_{3\times 3} & \boldsymbol{I}_{3\times 3} & \boldsymbol{0}_{3\times 3} \\ \boldsymbol{M} & \boldsymbol{N} & -\boldsymbol{R}_c^H \\ \boldsymbol{0}_{3\times 3} & \boldsymbol{0}_{3\times 3} & \boldsymbol{0}_{3\times 3} \end{bmatrix}, \\ &\boldsymbol{M} = \begin{bmatrix} 0 & 0 & 0 \\ 0 & -\omega_0^2 & 0 \\ 0 & 0 & 3\omega_0^2 \end{bmatrix}, \boldsymbol{N} = \begin{bmatrix} 0 & 0 & 2\omega_0 \\ 0 & 0 & 0 \\ -2\omega_0 & 0 & 0 \end{bmatrix}, \\ &\boldsymbol{B} = \begin{bmatrix} \boldsymbol{0}_{3\times 3} & \boldsymbol{R}_c^H & \boldsymbol{0}_{3\times 3} \end{bmatrix}^T, \\ &\boldsymbol{G} = \begin{bmatrix} \boldsymbol{0}_{3\times 3} & \boldsymbol{0}_{3\times 3} \\ -\boldsymbol{R}_c^H & \boldsymbol{0}_{3\times 3} \\ \boldsymbol{0}_{3\times 3} & \boldsymbol{I}_{3\times 3} \end{bmatrix}. \end{aligned} \tag{14}$$

The discrete system model can be written as

$$\boldsymbol{x}_{k+1} = \boldsymbol{\Phi}_{k+1,k}\boldsymbol{x}_k + \boldsymbol{\Psi}_{k+1.k}\boldsymbol{u}_k + \boldsymbol{\Gamma}_{k+1,k}\boldsymbol{w}_k\,, \tag{15}$$

where $\boldsymbol{\Psi}_{k+1.k} \approx T_s \cdot \boldsymbol{B}_k$ and $\boldsymbol{Q}_k = \mathrm{diag}\left[\sigma_{ax}^2\ \sigma_{ay}^2\ \sigma_{az}^2\ \sigma_{dx}^2\ \sigma_{dy}^2\ \sigma_{dz}^2\right]$, others are similar to those in AKF's.

The measurement equation of PKF can be written as

$$\boldsymbol{z}_{k+1} = \boldsymbol{H}_{k+1}\boldsymbol{x}_{k+1} + \boldsymbol{v}_{k+1}\,. \tag{16}$$

In (15), $\boldsymbol{z}_{k+1}$, expressed in $\{c\}$, represents relative position of the target with respect to the chaser from the VMU, i.e., $\boldsymbol{z}_{k+1} = \left[x^c, y^c, z^c\right]^T$. $\boldsymbol{v}_{k+1}$ is the measurement noise, whose covariance is $\boldsymbol{R}_{k+1} = \mathrm{diag}\left[\sigma_{x^c}^2\ \sigma_{y^c}^2\ \sigma_{z^c}^2\right]$. And the sensitivity matrix is $\boldsymbol{H}_{k+1} = \left[-\boldsymbol{R}_H^c\ \ \boldsymbol{0}_{3\times 3}\ \ \boldsymbol{0}_{3\times 3}\right]^T$.

IV. EXPERIMANT AND ANALYSIS

A. Numerical Simulation

The validity of the proposed information fusion algorithm based on Vision/IMU is verified in this subsection. An approaching trajectory of the two spacecraft is designed in accordance to a strategy for the RVD. Thus, the outputs of the IMU and VMU can be obtained by defining uncertainties showed in Section II.B. The parameters of simulations are set as shown in Table I.

TABLE I. SIMULATION PARAMETERS

Types	Parameters	Magnitudes	Units
Simulation Settings	Time	400	s
	Step	0.02	
VMU	Update frequency	6.25	Hz
	$\sigma_{x^c}\ \ \sigma_{y^c}\ \ \sigma_{z^c}$	0.033	m
	$\sigma_{\theta 1}\ \ \sigma_{\theta 2}\ \ \sigma_{\theta 3}$	0.005	deg
IMU	Update frequency	50	Hz
	$\varepsilon_x\ \ \varepsilon_y\ \ \varepsilon_z$	2.78×10^{-6}	deg/s
	$\sigma_{\varepsilon x}\ \ \sigma_{\varepsilon y}\ \ \sigma_{\varepsilon z}$	8.33×10^{-8}	
	$\sigma_{gx}\ \ \sigma_{gy}\ \ \sigma_{gz}$	8.33×10^{-7}	
	$d_x\ \ d_y\ \ d_z$	3.0×10^{-4}	m/s^2
	$\sigma_{dx}\ \ \sigma_{dy}\ \ \sigma_{dz}$	1.0×10^{-5}	
	$\sigma_{ax}\ \ \sigma_{ay}\ \ \sigma_{az}$	1.0×10^{-4}	

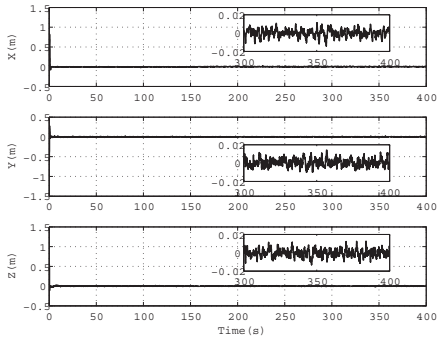

(a) Relative position

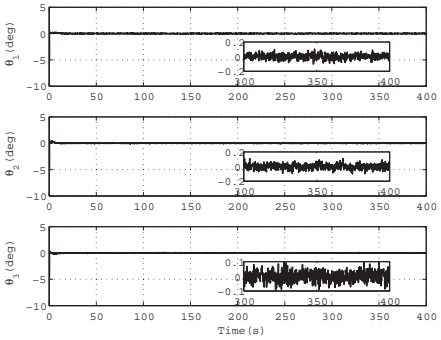

(b) Relative attitude

Figure 5. Estimation errors of fusion algorithm

Fig. 5 presents the estimation error of relative position and attitude after fusing the vision and inertial information. Apparently, these deviation variables are tending to converge to a region near the zero. More specifically, they are superior to 0.015 m and 0.12 deg respectively. The maximums (MAX) and standard deviations (SD) of the estimation errors, reported in Table II, show that estimation errors of relative position and attitude are reduced by 22% and 6% respectively, compared with measurement errors of the VMU, which indicates that the fusion algorithm base on Vision/IMU has better performance than using a single VMU.

TABLE II. MAXIMUMS AND STANDARD DEVIATIONS OF THE ESTIMATION ERRORS

Types	**Relative position** (m)			**Relative attitude** (deg)		
	ΔX	ΔY	ΔZ	$\Delta\theta_1$	$\Delta\theta_2$	$\Delta\theta_3$
MAX	0.0141	0.0142	0.0132	0.1078	0.1045	0.1146
SD	0.0037	0.0039	0.0039	0.0304	0.0315	0.0312

B. Semi-Physical Simulation

In order to validate the capability of the real-time measurement system, a semi-physical simulation in accordance with the semi-physical simulation closed loop was implemented based on the hardware-in-the-loop simulation system designed in Section II. The maneuver consists of autonomously following a planned path in front of the target and staying a ready state for a required time period. At this moment the chaser reaches the specified location and waits for a docking instruction.

The following requirements should be met in the process of the RVD.

- Control precision: referring to the Table III.
- Security: ensuring the chaser's safety during its approach to the target.
- Energy: avoiding unnecessary fuel consumption.
- Field of view: guaranteeing the observation of the target throughout the process.

TABLE III. CONTROL PRECISION IN READY PHASE

Control Variables	Constraints
Axial relative distance	0.4 ± 0.03 m
Axial relative velocity	±0.02 m/s
Radial relative distance	±0.02 m
Radial relative velocity	±0.02 m/s
Relative angular misalignment	< 0.5deg
Relative angular rate	< 0.1 deg/ s

Assume that the two spacecraft are relatively static at the beginning of docking. The influences of initial relative pose and measurement methods on docking accuracy are primarily considered. There are three schemes given in Table IV.

TABLE IV. INITIAL STATE AND MEASUREMENT METHOD

Scheme	Relative position (m)	Relative attitude (deg)	Measurement method
Scheme 1	(5, – 0.3, 0.3)	(3, 3, – 3)	Vision/IMU
Scheme 2	(10, – 0.5, 0.5)	(5, 5, – 5)	Vision/IMU
Scheme 3	(10, – 0.5, 0.5)	(5, 5, – 5)	Vision

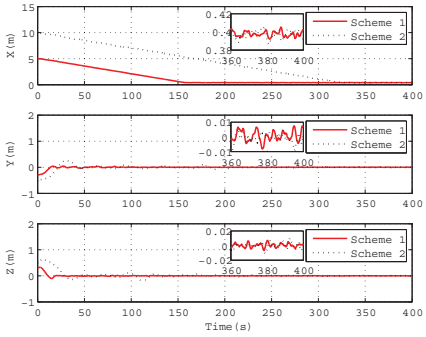

(a) Relative position

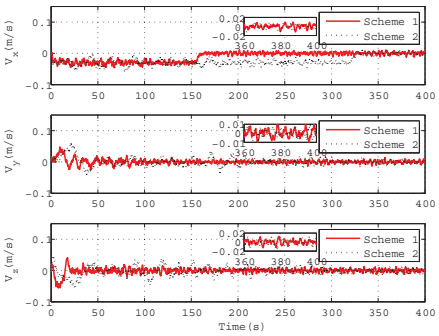

(b) Relative velocity

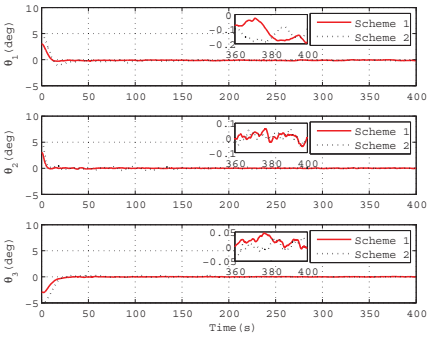

(c) Relative attitude

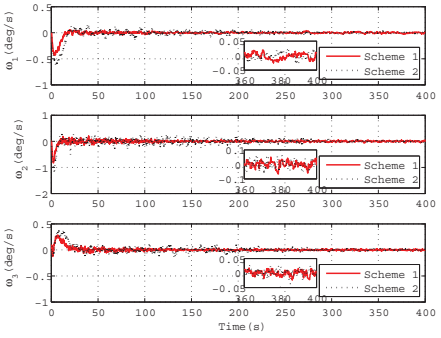

(d) Relative angular speed

Figure 6. Comparison of control variables in scheme 1 and 2

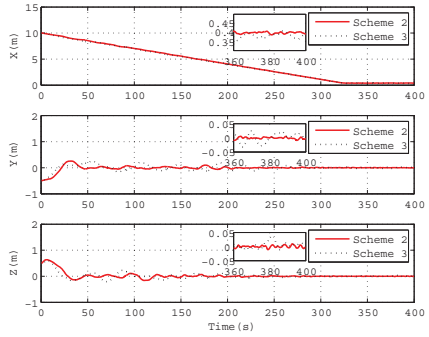

(a) Relative position

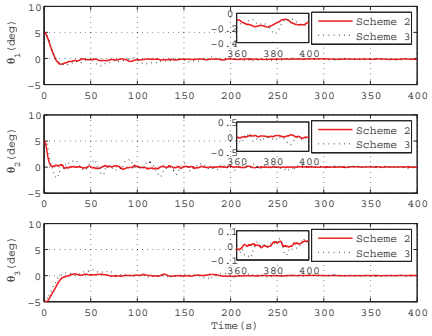

(b) Relative attitude

Figure 7. Comparison of the relative pose in scheme 2 and 3

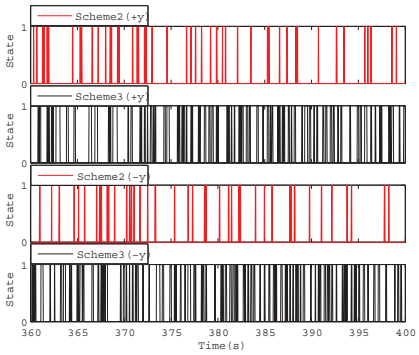

Figure 8. State of the torque engine along y -axis

Fig. 6 (a) depicts the evolution of relative distance in the process of autonomous proximity maneuver in scheme 1 and 2. The chaser follows a reference line toward the target, reaching the ready phase at time = 162 s and time =326 s respectively. The partial enlarged view shows that the axial distances are maintained in the range of 0.38 m ~ 0.42 m during the ready state. Fig. 6 (c) shows that relative attitudes, which almost converge to the expected values after time = 10 s, remain in the range of -0.3 deg ~ 0.1 deg for the rest of time. The curves of the relative velocity and angular speed, with overshoot and fluctuation in the first 40 seconds, are displayed in Fig. 6 (b) and (d).

In Table V, the maximal deviations of all the variables, including the relate position, velocity, attitude and angular speed from three schemes, are displayed. If any of them break the constraints in Table III, this means that the operation of the RVD is failed and the chaser needs to readjust its pose for the next docking. In scheme 1 and 2, all the control variables satisfy the precision demands in ready phase, referring to the Table III and V, which proves that the real-time measurement system has the capability of assisting the implementation of the autonomous RVD.

However, in Fig. 6, the fluctuations of control variables in scheme 1 is smaller in amplitude than the ones in scheme 2. e.g., the axial relative velocity of scheme 1 changes in the range of -0.05 m/s ~ -0.01 m/s, while scheme 2 in the range of -0.06 m/s ~ 0.01 m/s in the first 150 seconds. When a relative distance of 0.4 m is reached, their corresponding control variables have similar control precision. It is evident from these analyses that the magnitude of camera noise becomes larger with the growth of the relative distance.

Fig. 7 illustrates the evolution of relative pose in the process of the RVD in scheme 2 and 3. Obviously, the performance of pose control in scheme 3 is inferior to those in scheme 2. Specifically, in scheme 3, some control variables cannot meet the demands, referring to the Table V. e.g., both radial relative distances exceed the expectation, i.e., the range of -0.03 m ~ 0.03 m. These results indicate that the real-time measurement system has better navigation performance compared with visual sensors. At the time intervals 360 s < t < 400 s, the working time of torque engine along y -axis in scheme 2 is evidently shorter than the one in scheme 3, as shown in Fig. 8. Since the chaser does not regulate frequently for position and orientation, the real-time measurement system helps to save fuels. Therefore, in the case of close-range distance, it is essential to introduce the inertial information as the navigation reference to improve the navigation performance.

TABLE V. MAXIMAL DEVIATION OF CONTROL VARIABLES IN REDAY PHASE

Scheme	Relative position (m)			Relative velocity (m/s)			Relative attitude (deg)			Relative angular speed (deg/s)		
	X	Y	Z	V_x	V_y	V_z	θ_1	θ_2	θ_3	ω_1	ω_2	ω_3
Scheme 1	0.0053	-0.0081	0.0070	-0.0121	0.0100	-0.0127	-0.1945	0.0618	0.0455	-0.0250	-0.0660	-0.0245
Scheme 2	0.0064	-0.0093	-0.0111	-0.0128	-0.0094	-0.0182	-0.1881	-0.0583	0.0317	-0.0284	-0.0701	-0.0371
Scheme 3	0.0081	-0.0334	0.0392	-0.0169	0.0245	-0.0258	-0.2821	-0.2787	-0.0838	0.0667	0.2227	-0.0684

I. CONCLUSION

This paper has presented the design of real-time measurement system, which is an indispensable part of the semi-physical simulation system for an autonomous RVD. It is mainly composed of vision measurement system and inertial measurement system, with special attention to the fusion of the vision and inertial information. Simulations were conducted for two different approaches, one of which carried out numerical simulations to assess the effectiveness of information fusion algorithm. The second approach adopted semi-physical experiments, which can test the performance of real-time measurement system in the operation of the autonomous RVD. These results show that real-time measurement system is eligible to fulfil the expectation of the autonomous RVD in lunar orbit, and provides more precise and abundant navigation information, as well as less fuel consumption, compared with visual sensors.

REFERENCES

[1] Z. Z. Sun, Y. Jia, and H. Zhang, "Technological advancements and promotion roles of Chang'e-3 lunar probe mission (Periodical style)," *Science China (Technological Sciences)*, vol.56, no.11, pp. 2702–2708, November 2013.

[2] F. J. Pelletier, D. F. Golla, and A. C. M. Allen, "Lidar-based rendezvous navigation for MSR (Published Conference Proceedings style)," in *AIAA/AAS Astrodynamics Specialist Conference and Exhibit, Guidance, Navigation, and Control and Co-located Conferences*, Providence, Rhode island, 2004, pp. 2004-2018.

[3] J.W. McMahon, S. Gehly, and P. Axelrad, "Enhancing relative attitude and trajectory estimation for autonomous rendezvous using flash (Published Conference Proceedings style)," in *SPACE Conferences and Exposition*, San Diego, CA, 2014, pp. 4359-4374.

[4] J. F. Shi, S. Ulrich, S. Ruel, and M. Anctil, "Uncooperative spacecraft pose estimation using an infrared camera during proximity operations (Published Conference Proceedings style)," in *SPACE Conferences and Exposition*, Pasadena, California, 2015, pp. 4429-4445.

[5] F. Sansone, F. Branz, A. francesconi and M. Barbette, "2D close-range navigation sensor for miniature cooperative spacecraft (Periodical style)," *IEEE TRANSACTIONS ON AEROSPACE AND ELECTRONIC SYSTEMS*, vol. 50, no.1, pp. 160-169, Jan 2014.

[6] J. G. Li and H. T. Cui, "Vision-aided inertial navigation for pin-point landing on Mars (Published Conference Proceedings style)," in *International Conference on Intelligent Control & Information Processing*, 2011, pp.14-18.

[7] Z.You, Z. Luan and X. Wei, "Attitude disturbance correction for binocular vision cameras in rendezvous and docking (Periodical style)," *IEEE Aerospace & Electronic Systems Magazine*, vol.30, no.12, pp. 34-40, August 2015.

[8] T. Boge, T. Wimmer, O. Ma and M. Zebenay, "EPOS−A robotics-based hardware-in-the-loop simulator for simulating satellite RvD operations (Published Conference Proceedings style)," in *10th International Symposium on Artificial Intelligence, Robotics and Automation in Space*, Sapporo, Japan, 2010.

[9] M. Romano, D. A. Friedman and T. j. Shay, "Laboratory experimentation of autonomous spacecraft approach and docking to a collaborative target (Periodical style)," *Journal of Spacecraft & Rockets*, vol.44, no.1, pp.164-173, August 2006.

[10] S. C. Kim, J. L. Crassidis, Y. Cheng , A. M. Fosbury and J. L. Junkins, "Kalman filtering for relative spacecraft attitude and position estimation (Periodical style)," *Journal of Guidance Control & Dynamics*,vol.30, no.1, pp.133-143, 2007.